



Contents lists available at ScienceDirect

Marine and Petroleum Geology

journal homepage: www.elsevier.com/locate/marpetgeo

Seismic quality factors across a bottom simulating reflector in the Makran Accretionary Prism, Arabian Sea

Kalachand Sain*, Anoop Kumar Singh

National Geophysical Research Institute (Council of Scientific and Industrial Research), Uppal Road, Hyderabad 500 007, India

ARTICLE INFO

Article history:

Received 13 March 2010

Received in revised form

24 March 2011

Accepted 28 March 2011

Available online xxx

Keywords:

Seismic quality factor

Gas hydrates

Free-gas

Makran accretionary prism

ABSTRACT

The hydrate-bearing sediments above the bottom simulating reflector (BSR) are associated with low attenuation or high quality factor (Q), whereas underlying gas-bearing sediments exhibit high attenuation. Hence, estimation of Q can be important for qualifying whether a BSR is related to gas hydrates and free-gas. This property is also useful for identifying gas hydrates where detection of BSR is dubious. Here, we calculate the interval Q for three submarine sedimentary layers bounded by seafloor, BSR, one reflector above and another reflector below the BSR at three locations with moderate, strong and no BSR along a seismic line in the Makran accretionary prism, Arabian Sea for studying attenuation (Q^{-1}) characteristics of sediments. Interval Q for hydrate-bearing sediments (layer B) above the BSR are estimated as 191 ± 11 , 223 ± 12 , and 117 ± 5 , whereas interval Q for the underlying gas-bearing sediments (layer C) are calculated as 112 ± 7 , 107 ± 8 and 124 ± 11 at moderate, strong and no BSR locations, respectively. The large variation in Q is observed at strong BSR. Thus Q can be used for ascertaining whether the observed BSR is due to gas hydrates, and for identifying gas hydrates at places where detection of BSR is rather doubtful. Interval Q of 98 ± 4 , 108 ± 5 , and 102 ± 5 , respectively, at moderate, strong and no BSR locations for the layer immediately beneath the seafloor (layer A) show almost uniform attenuation.

© 2011 Elsevier Ltd. All rights reserved.

1. Introduction

Gas hydrates are crystalline form of methane and water, and are found in shallow sediments of outer continental margins where temperature is low; pressure is high and methane concentration exceeds the solubility limit (Kvenvolden, 1998; Sloan, 1998). They have attracted the scientific attention due to their natural occurrences; their role in climate change (methane being a green house gas) and submarine hazard that may cause slope failure; and most importantly their potential as future major energy resource (Booth et al., 1996; Klauda and Sandler, 2005; Sain and Gupta, 2008; Sain and Ojha, 2008). Hence, detection and quantitative assessment of gas hydrates are essential for evaluating the energy potential and assessing the environment-hazard. The commonly used proxy for gas hydrates is the bottom simulating reflector (BSR) that can be identified based on its characteristic features (Sain and Gupta, 2008) in seismic data. The BSR is an interface between gas hydrate-bearing sediments above and free-gas-saturated sediments below, which can be characterized by high seismic velocity for hydrate- and low

seismic velocity for gas-bearing sediments; high resistivity for both hydrate- and gas-bearing sediments; seismic blanking due to gas hydrates; high reflection strength and frequency shadow for the presence of gas (Ojha and Sain, 2009; Satyavani et al., 2008). Another important property to characterize the hydrate- and gas-bearing sediments is the seismic quality factor (Q) or attenuation (Sain et al., 2009). Estimation of Q is also required for compensating the effects of attenuation in the quest to improve the subsurface seismic images (Bellefleur et al., 2007); to better interpret the effects of amplitude variation with offset (AVO); and to invert seismic data for deriving material properties.

Gei and Carcione (2003) show in their model study that attenuation decreases or Q increases with increasing concentration of gas hydrates due to stiffening of sediments. In certain environments, fluids may be present within the gas hydrates stability zone, which show an increase in attenuation (Q^{-1}) for hydrate-bearing sediments (Guerin and Goldberg, 2002; Chand and Minshull, 2004; Priest et al., 2006). Matsushima (2006) demonstrated that hydrate-bearing sediments cause attenuation in the sonic frequency range (10–20 kHz), but not in the seismic frequency range (30–110 Hz). This leads to a scientific debate on the attenuation of gas hydrates. By employing the logarithmic spectral ratio (LSR) method to the surface seismic reflection data, Sain et al.

* Corresponding author.

E-mail address: kalachandsain@yahoo.com (K. Sain).

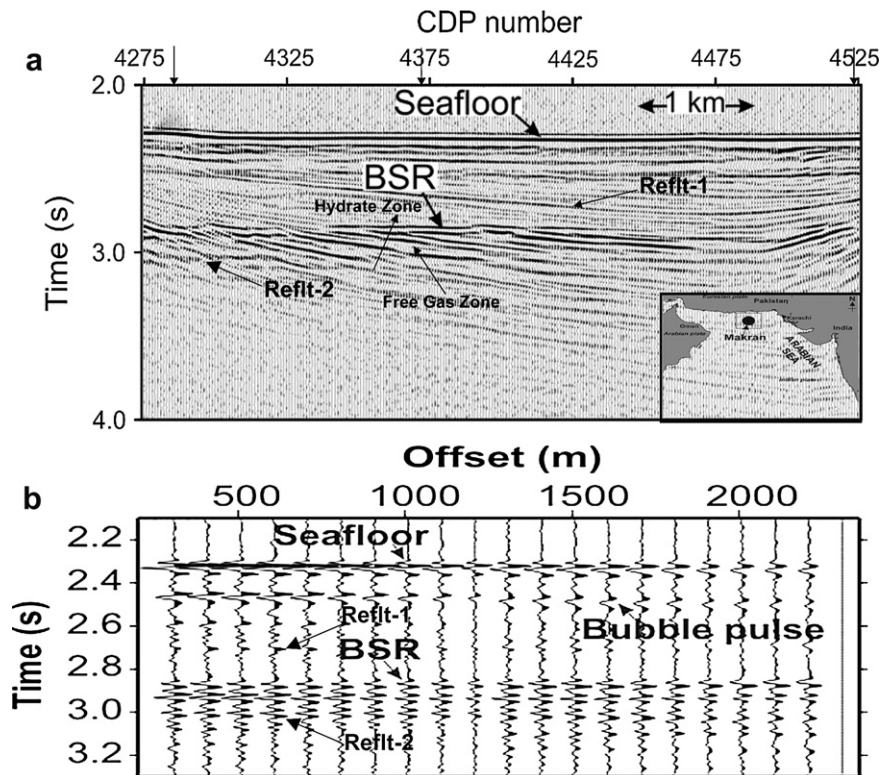


Fig. 1. (a). Seismic stack section along a north–south seismic line (inset shows the study area (box) in the Makran accretionary prism). Amplitude spectra have been calculated around four reflectors: seafloor, reflect-1, BSR and reflect-2. (b) NMO corrected CDP gather at CDP 4372, showing the reflections at various offsets from the said four reflectors.

(2009) demonstrated that the hydrate-bearing sediments are associated with high Q or low attenuation compared to that of normal (without hydrates) oceanic sediments.

The BSRs are wide-spread on seismic data in the Makran accretionary prism (Minshull et al., 1992; Sain et al., 2000). Studies of seismic attributes such as the blanking, reflection strength and

instantaneous frequency (Ojha and Sain, 2009) and the velocity anomaly (Sain et al., 2000) favor the presence of gas hydrates and free-gas across the BSR in the Makran offshore. Here we calculate the seismic Q at few CDP locations along a seismic line in the Makran accretionary prism with a view to understand the attenuation characteristics of gas hydrate- and free-gas-bearing sediments. The study

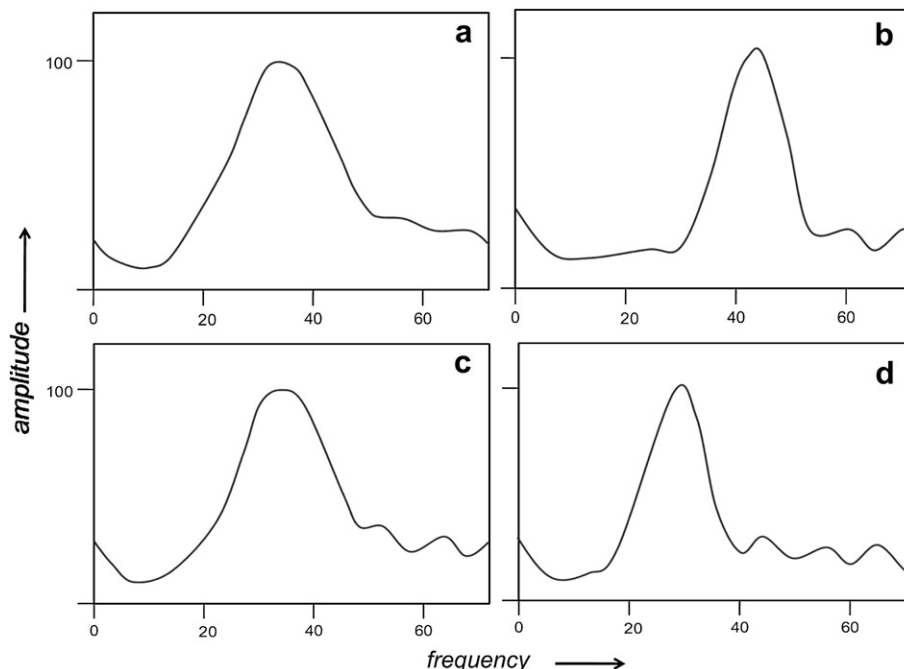


Fig. 2. Amplitude spectrum of a representative seismic trace at offset 300 m of CDP 4372 for sea floor (a), reflect-1 (b), BSR (c), and reflect-2 (d), respectively.

is useful to identify gas hydrates in the absence of well-identified BSR on seismic section, and to qualify whether an identified BSR is related to gas hydrates and underlying free-gas. Estimated Q can also be utilized for quantification of gas hydrates by establishing a relation between Q and saturation of gas hydrates like a relation that exists between the seismic velocity and saturation.

2. Methodology

The best known method for estimating Q from surface seismic reflection data of a 1-D multilayered earth is probably the LSR method (Sain et al., 2009) where logarithm of spectral ratio of vertical reflections from two different reflectors with reflection times t_1 and t_2 (Bath, 1974) is calculated as

$$\ln \frac{|A(f)_2|}{|A(f)_1|} = \ln \frac{G_2 |C_2(f)|}{G_1 |C_1(f)|} - \pi \left[\frac{t_2}{Q_{av2}} - \frac{t_1}{Q_{av1}} \right] f \quad (1)$$

Subscripts 1 and 2 denote the first and second layers, respectively. G accounts for the geometrical spreading and C takes into account the effects of reflection and transmission at boundaries.

Q_{av2} and Q_{av1} are the average Q from the source to the first and second layers, respectively. The LSR against f as per Eq. (1) represents a straight line with slope, m as

$$m = -\pi \left[\frac{t_2}{Q_{av2}} - \frac{t_1}{Q_{av1}} \right] \quad (2)$$

From above equation we derive Q_{av2} as

$$Q_{av2} = \frac{\pi t_2 Q_{av1}}{\pi t_1 - m Q_{av1}} \quad (3)$$

The average and interval Q for the first layer is the same and thus we can calculate the Q_{av2} from Eq. (3). The Q between t_2 and t_1 , defined as the interval quality factor, Q_{int} , can be calculated using the equation of Zhang and Ulrych (2002) as

$$Q_{int} = \frac{t_2 - t_1}{Q_{av2}^{-1} t_2 - Q_{av1}^{-1} t_1} \quad (4)$$

Following this LSR method, we can calculate the Q_{int} for all subsequently deeper layers for a multilayered earth.

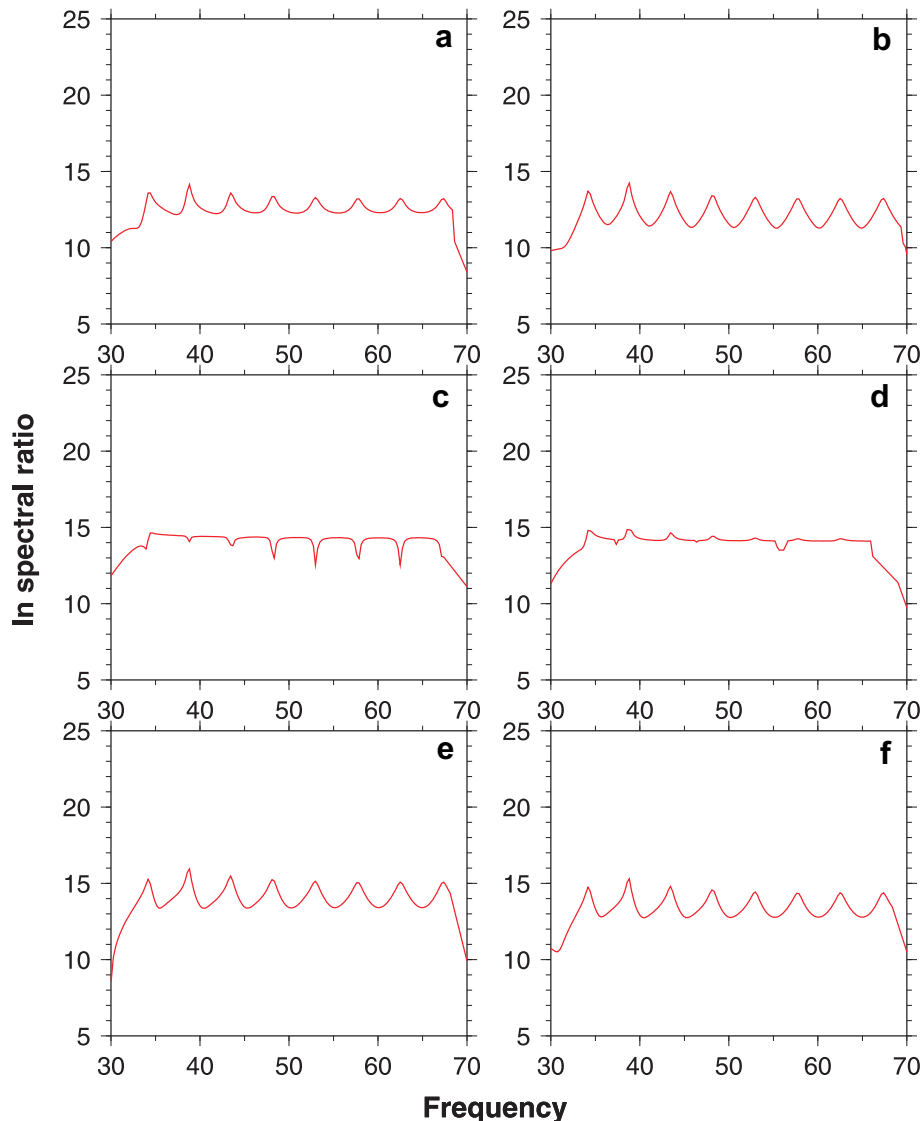


Fig. 3. Natural logarithms of spectral ratio with reference to seafloor at representative offsets of 500 and 2000 m for reflect-1 (a–b), BSR (c–d), and reflect-2 (e–f), respectively, for CDP 4372.

3. Application and results

We use the CDP gathers from field seismic data to calculate Q_{int} at various locations with moderate, strong, and no BSR (Fig. 1a) along a seismic line located in the Makran accretionary prism. This profile shows BSR at about 2.85–2.9 ms two way time (TWT) beneath the seafloor with water depth of ~ 2.3 s TWT in the Makran accretionary prism (Minshull et al., 1992; Sain et al., 2000). The section is north–south oriented and the CDP number increases landward. The CDP has 24 traces with 100 m separation, and the nearest trace lies at 200 m offset. The sampling rate of the data is 4 ms. Since the last three traces are noisy, we have muted them. The conventional seismic data processing had been done using PROMax-2D and the sequence included a bandpass filter (4–8–50–60 Hz), spherical divergence correction ($1/(\text{time} \times \text{velocity}^2)$), minimum phase spiking deconvolution, detailed velocity analysis at every 10th CDP intervals, normal moveout (NMO) correction and trace equalization. Hydrophone array attenuation was corrected using the function of Sheriff and Geldert (1995). No source array correction was applied because it was considered as a point source (Sain et al., 2000).

The LSR method is valid for vertically traveling seismic wave. Since the first trace of a CDP gather is at 200 m offset, which is often associated with the shot generated noise, the Q estimated from the nearest trace of a multi channel seismic (MCS) data may not be reliable. We apply the LSR method to all offsets of the NMO corrected raw CDP gather without any filtering. At increasing offsets, the actual path lengths of seismic waves through the sediments increase, while the apparent path lengths derived from the arrival times of the seafloor and any deeper reflector decrease due to different receiver positions and ray paths. Thus, estimated average Q at offset (x), Q_x falls with increasing offset. Sain et al. (2009) showed that Q_x decreases exponentially with offset as

$$\ln Q_x = \ln Q_0 - kx \quad (5)$$

where k is assumed to be constant over the range of a CDP and Q_0 is the average Q at zero-offset for the vertically traveling wave, which we are looking for. By calculating average Q_x at all offsets as per Eq. (3) and then extrapolating back to zero-offset as per Eq. (5), we can determine the desired average Q_0 from the surface seismic reflection data.

We employ the approach to an NMO corrected raw seismic gather (Fig. 1b) at CDP 4372 where the BSR is very strong. We calculate the amplitude spectra by the Fast Fourier Transformation (FFT) using a Hamming window function within a time window of 100 ms for four reflectors at seafloor, reflect-1 below the seafloor, the BSR and reflect-2 below the BSR. While calculating the amplitude spectrum using a time window, one has to take care that the window should contain a reflector only and must not straddle over other reflection event. As per the full-waveform inversion result (Sain et al., 2000) of MCS data in the study region, we can expect minimum separation of 100 ms two way time between two consecutive reflectors. We have chosen 100 ms time window in such a way that the window just contain the reflector. The window is not centered on the reflections (sea floor, reflect-1, BSR and reflect-2). As far as meaning of Q at BSR is concerned, we calculate the amplitude spectrum of the window containing the BSR only (not centered around BSR), giving rise to Q for the layer above the BSR. (Fig. 2) displays the amplitude spectra of a representative trace at offset 300 m of CDP 4372 for 4 reflections to show the overall quality of data prior to the spectral ratio calculation.

The LSR method requires the source signature. Since the attenuation ($Q=10,000$) through the water column is almost negligible, we can assume the seafloor reflection as a reference signal in absence of source signature. Natural logarithms of spectral ratios of reflections from reflect-1, BSR and reflect-2 with reference

to the seafloor reflection are used for calculating the slopes as per Eq. (1). (Fig. 3) shows the representative LSR from reflect-1 (a, b), BSR (c, d), Reflect-2 (e, f) at near (500 m) and far (2000 m) offsets, respectively. It is to be mentioned here that as Q is independent of frequency (Aki and Richard, 1980), only the flat portions of the spectral ratios are used for the calculation of Q . We observe the wavy spectral ratio for field data that has also been observed by Dasgupta and Clark (1998) for the estimation of attenuation or seismic Q . Since the Q for water and the reflection times of seafloor, reflect-1, BSR and reflect-2 are known, the average Q_x at an offset, x upto reflect-1, BSR and reflect-2 can be calculated using Eq. (3). By extrapolating back to zero-offset according to Eq. (5), we can calculate the average Q_0 (Fig. 4) up to the reflect-1, BSR, reflect-2. The errors in field data are mapped into mean error, $\delta(Q_0)$ in estimated average Q_0 , which is determined according to following equation derived by Sain et al. (2009)

$$\delta(Q_0) = Q_0 \delta(\ln Q_0) \quad (6)$$

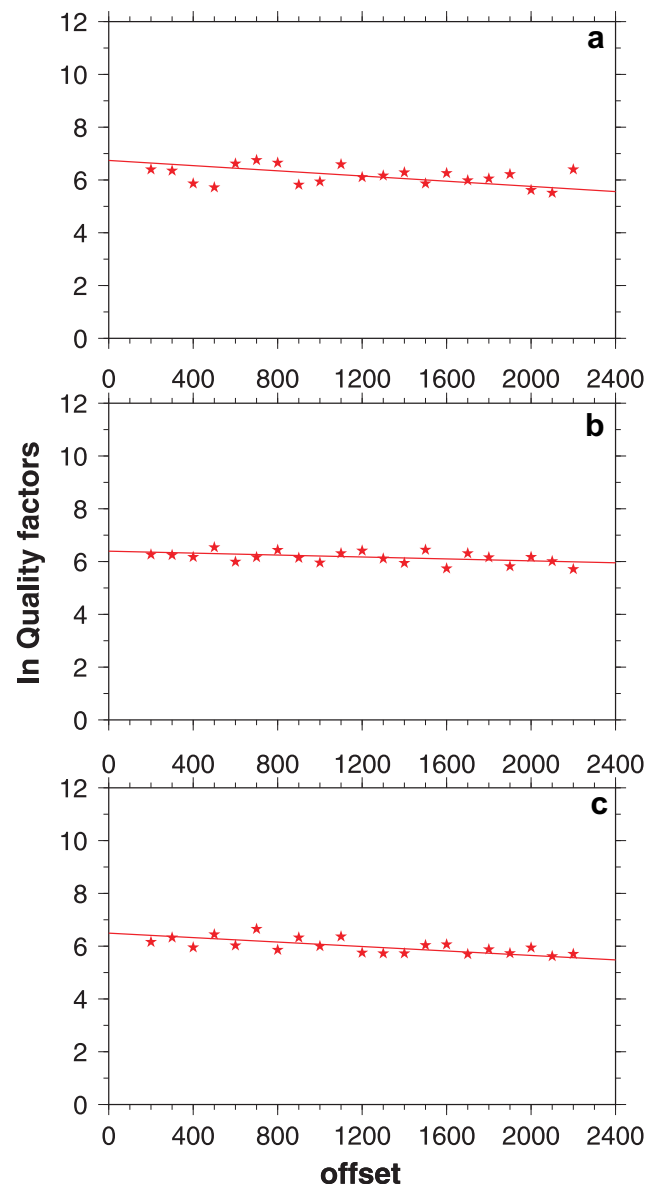


Fig. 4. Natural logarithm of average Q_x versus offsets for CDP 4372 to calculate average Q_0 up to reflect-1, BSR, and reflect-2, respectively.

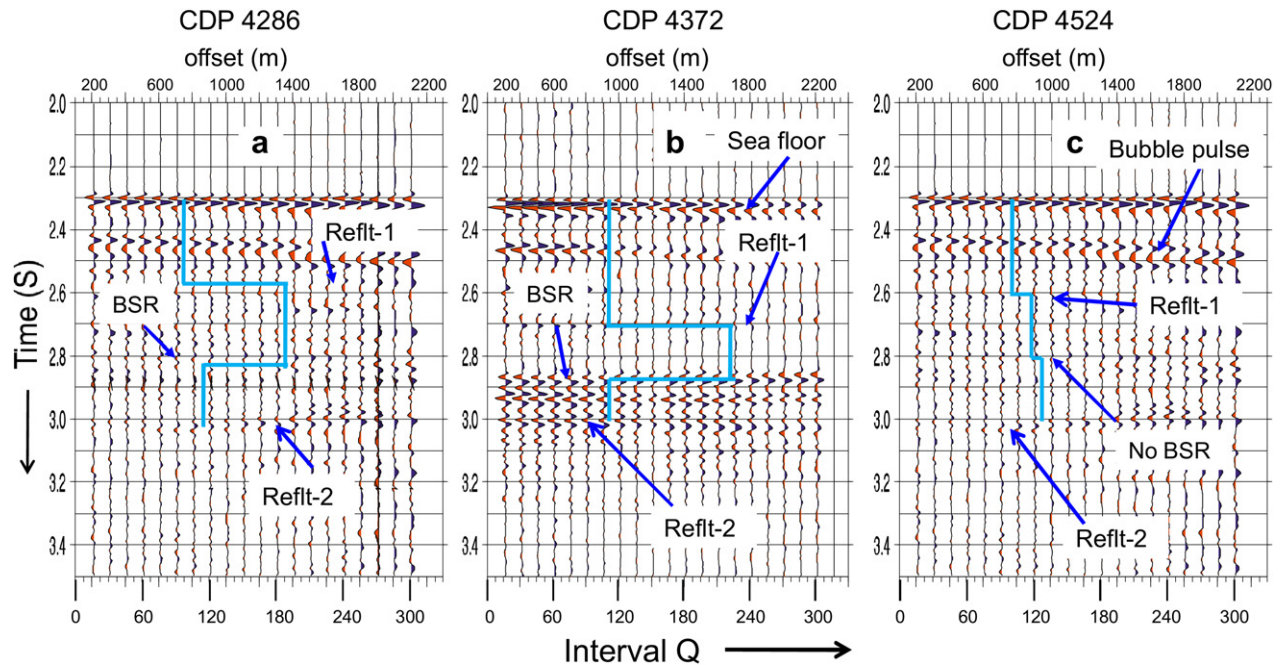


Fig. 5. Field seismic gathers at CDPs 4286, 4372, and 4524, respectively, each superimposed with estimated interval Q .

The Q_{int} between two successive reflectors is then calculated using the Eq. (4). The mean error, $\delta(Q_{\text{int}})$ in estimated Q_{int} is then determined using the following equation as

$$\delta Q_{\text{int}} = \frac{(t_2 - t_1) (Q_{\text{av1}}^2 t_2 \delta Q_{\text{av2}} - Q_{\text{av2}}^2 t_1 \delta Q_{\text{av1}})}{(t_2 Q_{\text{av1}} - t_1 Q_{\text{av2}})^2} \quad (7)$$

The interval Q and associated error for sedimentary formations between seafloor to reflect-1 (layer A), reflect-1 to BSR (layer B), and BSR to reflect-2 (layer C) at strong BSR (CDP 4372) are calculated as 108 ± 5 , 223 ± 12 , and 107 ± 8 , respectively. For comparison we select the CDP 4286 and 4524 where the BSR is moderate and absent, respectively. The interval Q and associated error for sedimentary layers bounded by these reflectors are calculated as 98 ± 4 (layer A), 191 ± 11 (layer B) and 112 ± 7 (layer C) at moderate BSR, and 102 ± 5 (layer A), 117 ± 5 (layer B), and 124 ± 11 (layer C) at no BSR locations, respectively. The estimated Q in the hydrate-bearing sediment is comparable to Q estimated for hydrate-bearing sediments in other environments (Petersen et al., 2007; Sain et al., 2009). The interval Q versus TWT 1-D models are superimposed in (Fig. 5) over the respective CDP gathers from which the interval Q are derived using the LSR method. By placing these 1-D models at appropriate locations along the seismic line, we can produce a pseudo 2-D Q structure in the study region.

4. Discussion and conclusions

We have applied the LSR method to calculate Q_{int} from marine MCS reflection data at three locations where the BSR is moderate, strong and absent along a seismic line in the Makran accretionary prism. The study reveals a three-layered Q structure of shallow submarine sediments, which varies both laterally and vertically. The Q_{int} of the layer A shows almost uniform variation from 98 to 108 to 102 at CDPs 4286, 4372 and 4524, respectively, along the seismic line. We observe a large lateral change in Q_{int} for the layer B from 191 to 223 to 117 at locations where the BSR is moderate, strong and absent. We estimate the Q_{int} as 102, 117 and 124 for

layers A, B and C, respectively, at CDP 4524 where the BSR is absent. This gradual increase of Q_{int} downward can be considered as the background (without gas hydrates and free-gas) Q due to increase in pressure. Near the strong BSR at CDP 4372, we find a sudden increase in Q_{int} from 108 (layer A) to 223 (layer B), followed by a large drop in Q_{int} to 107 (layer C). This can be explained by the presence of good amount of gas hydrates above and free-gas below the BSR. The moderate BSR at CDP 4286 is associated with moderate increase in Q_{int} from 98 (layer A) to 191 (layer B), followed by a drop to 112 (layer C). This may indicate moderate amount of gas hydrates and less amount of free-gas across the BSR. In this paper, we attribute the high Q or low attenuation above, and low Q or high attenuation below the BSR, are due to gas hydrates and free-gas, which is supported by the 200–350 m thick low velocity (1.3–1.5 km/s) ‘free-gas’ zone beneath 160 m thick high velocity (2.0–2.2 km/s) gas hydrate-bearing sediments across the BSR, which are estimated by the full-waveform inversion of MCS data at CDPs 4375 and 4400 along the same seismic line in the Makran accretionary prism (Sain et al., 2000). Computation of seismic blanking above the BSR, and high reflection strength and frequency shadow below the BSR along the same line also imply the presence of gas hydrates and free-gas across the BSR (Ojha and Sain, 2009).

The calculation of Q can explain the relative strength of BSR along the seismic line in the study region. Since we do not observe high attenuation (Q^{-1}) in the hydrate-bearing sediments, as have been observed by many scientists (Guerin and Goldberg, 2002; Chand and Minshull, 2004; Priest et al., 2006), we can conclude that the fluids may not coexist with gas hydrates in the Makran accretionary prism. The study of attenuation is also useful for detection of gas hydrates in areas where identification of BSR becomes rather difficult due to parallel bedding. We intend to establish a relation between the saturation and Q for translating the increase and reduction of Q against the background value in terms of saturation of gas hydrates and free-gas. Besides characterizing the sediments, the estimated Q can be used for designing an inverse Q filter to compensate the effects of attenuation for producing improved structural images of shallow submarine sediments including the BSR and other reflectors.

Acknowledgements

The authors are grateful to the Director, NGRI for his permission to publish this work. We thank the Ministry of Earth Sciences, Govt. of India for sponsoring the gas hydrates research at NGRI. We are thankful to two anonymous reviewers for constructive suggestions and comments to improve our work.

References

- Aki, K., Richard, P.G., 1980. *Quantitative Seismology, Theory and Method*. W.H. Freeman and Company, pp. 167–185.
- Bath, M., 1974. *Spectral Analysis in Geophysics*. Elsevier Science Publishing Company, Inc, pp. 333–346.
- Bellefleur, G., Riedel, M., Brent, T., Wright, F., Dallimore, S.R., 2007. Implication of seismic attenuation for gas hydrate resource characterisation, Mallik, Mackenzie Delta. *Canadian Journal of Geophysical Research* 112, B10311.
- Booth, J.S., Rowe, M.M., Fischer, K.M., 1996. *Offshore Gas Hydrate Sample Database with an Overview and Preliminary Analysis*. U.S. Geological Survey, Open-File Report 96–272, 1 p.ate, pp. 31.
- Chand, S., Minshull, T.A., 2004. The effect of hydrate content on seismic attenuation – a case study from Mallik 2L-38 well data, MacKenzie Delta, Canada. *Geophysical Research Letters* 31, L14609.
- Dasgupta, R., Clark, R.A., 1998. Estimation of Q from surface seismic reflection data. *Geophysics* 63, 2120–2128.
- Gei, D., Carcione, J.M., 2003. Acoustic properties of sediments saturated with gas hydrate, free gas and water. *Geophysical Prospecting* 51, 141–157.
- Guerin, G., Goldberg, D., 2002. Sonic waveform attenuation in gas hydrate-bearing sediments from the Mallik 2L-38 research well, Mackenzie Delta. *Canadian Journal of Geophysical Research* 107, 2088.
- Klauda, J.B., Sandler, S.I., 2005. Global distribution of methane hydrate in ocean sediment. *Energy and Fuels* 19, 459–470.
- Kvenvolden, K.A., 1998. A primer on the geological occurrence of gas hydrate. In: Henriot, J.P., Mienert, J. (Eds.), *Gas Hydrates: Relevance to the World Margin Stability and Climate Change*. Geological Society of London, Special Publications, vol. 137, pp. 9–30.
- Matsushima, J., 2006. Seismic attenuation in methane-hydrate-bearing sediments: vertical seismic profiling data from the Nankai Trough exploratory well, offshore Tokai, central Japan. *Journal of Geophysical Research* 111, B10101.
- Minshull, T.A., White, R.S., Barton, P.J., Collier, J.S., 1992. Deformation at plate boundaries around the Gulf of Oman. *Marine Geology* 104, 265–277.
- Ojha, M., Sain, K., 2009. Seismic attributes for identifying gas hydrates and free-gas zones: application to the Makran accretionary prism. *Episodes* 32, 264–270.
- Petersen, C.J., Papenberg, C., Klaeschen, D., 2007. Local seismic quantification of gas hydrates and BSR characterization from multi-frequency OBS data at northern Hydrate Ridge. *Earth and Planetary Science Letters* 255, 414–431.
- Priest, J.A., Best, A.I., Clayton, C.R.I., 2006. Attenuation of seismic waves in methane gas hydrate-bearing sand. *Geophysical Journal International* 164, 149–159.
- Sain, K., Minshull, T.A., Singh, S.C., Hobbs, R.W., 2000. Evidence for a thick free gas layer beneath the bottom simulating reflector in the Makran accretionary prism. *Marine Geology* 164, 3–12.
- Sain, K., Gupta, H.K., 2008. Gas hydrates: Indian scenario. *Journal of Geological Society of India* 72, 299–311.
- Sain, K., Ojha, M., 2008. Identification and quantification of gas hydrates: a viable source of energy in the 21st century. *Memoir Geological Society of India* 68, 273–288.
- Sain, K., Singh, A.K., Thakur, N.K., Khanna, R.K., 2009. Seismic quality factor observations for gas hydrate-bearing sediments on western margins of India. *Marine Geophysical Researches* 30, 137–145.
- Satyavani, N., Sain, K., Lall, M., Kumar, B.J.P., 2008. Seismic attribute study for gas hydrates in the Andaman offshore, India. *Marine Geophysical Researches* 29, 167–175.
- Sheriff, R.E., Geldert, L.P., 1995. *Exploration Seismology: History, Theory, Data Acquisition*, vol. 1. Cambridge University Press, New York.
- Sloan, E.D., 1998. *Clathrate Hydrate of Natural Gases*. Marcel Dekker, New York.
- Zhang, C., Ulrych, T.J., 2002. Estimation of Q from CMP records. *Geophysics* 67, 1542–1547.